

Impact of Gd-, La-, Nd- and Y-Doping on the Textural, Electrical Conductivity and N₂O Decomposition Activity of CuO Catalyst

Bahaa M. Abu-Zied^{1,*}, Salem M. Bawaked², Samia A. Kosa², Wilhelm Schwieger³

¹ Center of Excellence for Advanced Materials Research (CEAMR), King Abdulaziz University, P.O. Box 80203, Jeddah 21589, Saudi Arabia

² Chemistry Department, Faculty of Science, King Abdulaziz University, P.O. Box 80203, Jeddah 21589, Saudi Arabia

³ Institut Für Chemische Reaktionstechnik, Friedrich-Alexander-Universität Erlangen-Nürnberg, Egerlandstraße 3, 91058 Erlangen, Germany

*E-mail: babuzaid@kau.edu.sa

Received: 14 December 2015 / Accepted: 5 January 2016 / Published: 1 February 2016

In this paper, a series of rare earth (Gd, La, Nd, and Y) doped CuO catalysts have been successfully prepared by using the microwave assisted co-precipitation method and tested for N₂O direct decomposition. The decomposition pathway of the catalysts precursors was followed up using thermogravimetric analysis (TGA). Several physico-chemical techniques were used in the characterization of the obtained catalysts including XRD, FT-IR, FE-SEM, TEM, N₂ adsorption, XPS, and H₂-TPR. Structural analysis revealed the formation of nanocrystalline monoclinic CuO as a major phase in all the prepared catalysts together with minor amount of the rare earth oxides. FE-SEM and TEM observations revealed the smaller crystallites sized of the rare earth-containing catalysts compared to the bare CuO one. All the rare earth-doped CuO catalysts showed higher activity and improved electrical conductivity compared to the bare CuO. The activity enhancement of the added rare earth oxides were discussed in terms of the electrical conductivity as well as the structural characterization results.

Keywords: Greenhouse gases, N₂O decomposition, electrical conductivity, nitrous oxide, CuO catalyst, rare earth promoted-CuO

1. INTRODUCTION

Due to the harmful effects of nitrous oxide (greenhouse gas, contributes to the stratospheric ozone destruction, and causes the acid rains) a growing attention has been focused on finding solutions

for its abatement. The catalytic route represents the most important strategy and successful solution for this environmental problem [1].

Before addressing the harmful effects of nitrous oxide, N_2O decomposition was used for the first time at the fifties and sixties to evaluate the activity of metal oxide catalysts [2]. The activity of the metal oxides depends on the oxidation state of the elements. In this way, the following activity order (per unit surface area) was reported over manganese oxides: $MnO < Mn_3O_4 < MnO_2 < Mn_2O_3$ [3], thus it seems that the 3+ is optimal oxidation state. For vanadium, it was found that 3+ oxidation state, i.e. V_2O_3 , is much more active than the 5+ oxidation state (V_2O_5) which is nearly inactive [4]. Also CoO was reported to exhibit very low activity compared to Co_3O_4 [5,6].

Supported oxides have been investigated, too, for N_2O decomposition. For instance, Tuti et al. [7] have investigated the activity of cobalt, copper, and iron oxides supported on zirconia. The following activity order was obtained: $Co_x/ZrO_2 > Cu_x/ZrO_2 \gg Fe_x/ZrO_2$. Moreover, the decomposition rate was found to be directly proportional to the metal content up to 2.3, 2.5, and 3.8 atoms nm^{-2} for Co, Cu, and Fe atoms, respectively. The activity of all catalysts was inhibited in the presence of O_2 and H_2O . However, the elimination of such additive has led to a recovery of the N_2O decomposition activity. Yao et al. [8] have investigated the influence of the preparation method on the activity of CuO/Al_2O_3 catalysts. They concluded that, the specific activity of the catalyst prepared by the multiple grafting is more active than the catalysts prepared by conventional wet impregnation and by mechanical mixing. In contrast to the catalysts prepared by the latter two methods, the activity of the catalyst prepared via the multiple grafting procedure was shown to be sensitive to copper loading.

The activity of metal oxides towards N_2O decomposition was reported to be greatly enhanced on doping with alkali cations. In this regard, Pasha et al. [9] reported a promotion effect during N_2O decomposition on doping NiO with Cs-ions. The optimal Cs/Ni ratio was 0.10. The promotion effect of Cs-ions was ascribed to their role in enhancing the Ni–O bond strength, which in turn facilitates the oxygen desorption under catalytic conditions [9]. The same research group has investigated the influence of Cs-doping on the activity of CuO catalyst (Cs/Cu = 0.05, 0.10, 0.15, and 0.20) [10]. It was found that all the Cs promoted catalysts were more active than the un-promoted bulk CuO, where the highest activity was obtained over the catalyst with the Cs/Cu ratio of at 0.1. Moreover, all promoted catalysts showed a better performance in the presence of O_2 and/or H_2O in the feed. Using a series of characterization techniques these authors have related the promotion effect of Cs ions to their role in improving the reduction of $Cu^{2+}-Cu^0$, thus facilitating the desorption of adsorbed oxygen species formed during the N_2O decomposition [10].

The measurements of the electrical conductivity of solid oxide catalysts can yield useful information about the nature of interaction between the solid oxide and its support, the redox features of the active phase under reaction conditions, the presence of charged oxidizing species, the nature of surface defects, etc. [11,12]. Therefore, the combination of the electrical conductivity of oxides catalysts with their catalytic activities can help in understanding their catalytic performances. The correlation between the electrical conductivity of various catalytic systems and their activity profiles has already been reported by many research groups [11–14]. In this way, Madeira et al. [11] reported that doping $NiMoO_4$ with cesium ions has led to an increase of its electrical conductivity. Consequently, a substantial decrease of the apparent activation energy of conduction was obtained.

Such conductivity promotion was correlated with the higher selectivity of the Cs-promoted NiMoO₄ during oxidative dehydrogenation (ODH) of *n*-butane [11]. Concurrently, employing a sequences of electrical conductivity experiments under different gaseous atmosphere Viparelli et al. [12] established a dependence of the redox character and the propane ODH performance of a series of TiO₂-supported vanadia–niobia catalysts. Recently, Popescu et al. [14] correlated the catalytic behavior of a series of LaCo_{1-y}O₃ (*y* = 0 and 0.2) and LaCo_{1-x}Fe_xO₃ (*x* = 0.6 and 1) perovskites for the total oxidation of methane and their conducting behavior. The N₂O decomposition activity was correlated with the in situ electrical conductivity decrease over transition metal exchanged ZSM-5 [15] and X [16] zeolites.

With respect to the influence of rare earth oxides dopants in promoting the N₂O decomposition over CuO catalysts, Konsolakis et al. [17] reported a promotion effect of CeO₂ addition during N₂O decomposition over CuO, where a complete conversion was achieved at 550 °C. More recently, we have reported the role of Pr-, Sm- and Tb-oxides in enhancing electrical conductance and the reduction of CuO as N₂O decomposition catalysts [18]. In a continuation of that work, we report in this paper the promotion effect of another series of rare earth (RE) oxides (Gd, La, Nd and Y) during N₂O decomposition over CuO catalyst. The different catalysts were prepared by the microwave assisted method of copper and RE oxalates and the subsequent calcination at 500 °C. The obtained catalysts were characterized by using a variety of physicochemical techniques including TGA, XRD, FTIR, FE-SEM, TEM, H₂-TPR, XPS and N₂-sorption analyses. The promotion effect of the added RE-oxides was discussed in terms of the observed electrical conductivity and reduction behavior of CuO enhancement.

2. EXPERIMENTAL

2.1. Catalysts preparation

Analytical grade copper nitrate (Cu(NO₃)₂·3H₂O), gadolinium nitrate (Gd(NO₃)₃·6H₂O), lanthanum nitrate (La(NO₃)₃·6H₂O), neodymium nitrate (Nd(NO₃)₃·6H₂O), yttrium nitrate (Y(NO₃)₃·6H₂O), cetyltrimethylammonium bromide (CTAB) and oxalic acid (H₂C₂O₄) were used in the catalysts preparations. The various RE/CuO catalysts were prepared by the microwave assisted coprecipitation method employing a microwave power (MWP) of 280 W [18,19]. Briefly, the required amounts of copper nitrate and RE nitrate, a using RE/Cu ratio of 0.05, were dissolved in distilled water. A solution containing CTAB was then added to the nitrates solution and mixed well. The precipitant solution, oxalic acid, was then added with constant stirring. The obtained mixture was immediately placed in a domestic microwave for 10 min at a MWP of 280 W. The resulted precipitate was cooled to room temperature and, then, washed and separated by using successive centrifugation. The various RE/Cu-oxalated were dried overnight at 55 °C. Finally, based on the TGA analysis (vide infra), the dried precipitates were calcined for 1 h in air at 500 °C to produce the various RE/CuO catalysts.

2.2. Characterization techniques

The structure of the obtained materials was investigated at ambient temperature using Thermo-Scientific ARL X'TRA Powder Diffractometer. The weight change accompanying the heating of the prepared RE/Cu-oxalates was followed using thermogravimetric analysis (TGA) using a TA instrument apparatus (model TGA-Q500) at a heating rate of $10\text{ }^{\circ}\text{C min}^{-1}$ in nitrogen flow (40 ml min^{-1}). The weight of the sample taken in each run was around 5 mg. FT-IR spectra were performed on Nicolet iS50 FT-IR spectrometer using Attenuated Total Reflectance (ATR) sampling accessory. The morphology and particles size of the prepared RE/CuO catalysts were investigated by using transmission electron microscopy (TEM) using JEOL (model JEM1011) microscopy and field emission scanning electron microscope (FE-SEM) on a JEOL model JSM-7600F microscope. The electrical conductivity measurements of the RE/CuO catalysts was performed using a Pyrex glass cell. In each experiment a 0.5 g of the catalyst powder was placed between two silver electrodes having 1.0 cm diameter. The resistance measurements were carried out using Keithley 6517A electrometer. Hydrogen temperature-programmed reduction (H_2 -TPR) patterns were constructed using Quantachrome CHEMBET-3000 instrument operated with a TCD detector. Prior to the measurements, the sample was pre-treated in helium at $300\text{ }^{\circ}\text{C}$ for 30 min then cooled to $25\text{ }^{\circ}\text{C}$. The flow of the gas was, then, changed to $5\% \text{ H}_2 + 95\% \text{ Ar}$ and the sample temperature increased to $600\text{ }^{\circ}\text{C}$ at the rate of $5\text{ }^{\circ}\text{C min}^{-1}$. Nitrogen adsorption measurements, at $-196\text{ }^{\circ}\text{C}$, were performed using an automated nitrogen adsorption apparatus (QUADRASORB evo, Quantachrome Co.). Prior to the analysis, each catalyst was degassed at $250\text{ }^{\circ}\text{C}$ for 12 h. XPS spectra were acquired using a SPECS GmbH X-ray photoelectron spectrometer with a standard dual-anode excitation source emitting monochromatic Al-K α (1486.6 eV) radiation operated at 13.5 kV and $5 \times 10^{-10}\text{ mbar}$.

2.3. Activity measurements

N_2O direct decomposition experiments were performed using a continuous flow quartz-glass reactor, at atmospheric pressure, containing approximately 0.5 g of the RE/CuO catalyst at a temperature range of 150 and $500\text{ }^{\circ}\text{C}$ and a W/F value of 0.15 g s cm^{-3} . The inlet nitrous oxide gas flow was introduced onto the catalyst bed from the bottom. The reactor was heated electrically using a temperature-controlled furnace, where the catalyst temperature inside the reactor was measured using a thermocouple on the catalyst bed. In each experiment, the catalyst was first pretreated at $500\text{ }^{\circ}\text{C}$ in helium for 1 h. N_2O , 500 ppm, was introduced to the catalyst bed with the aid of Bronkhorst thermal mass flow controllers using helium as a balance gas. Non-dispersive infrared analyzer (Hartmann and Braun, Uras 10E) was used to measure the N_2O inlet and outlet concentrations.

3. RESULTS AND DISCUSSION

3.1. Catalysts Characterization

The obtained FT-IR spectra of the as prepared RE/Cu oxalates, in the spectral range between 4000 and 400 cm^{-1} , are shown in Fig. 1(A). It is evident that the four samples exhibit the same

absorption peaks. The absorption appear at 505 cm^{-1} could be related to the $\nu(\text{Cu-O})$ vibration mode, whereas the peak at 825 cm^{-1} could be assigned to $\delta(\text{O-C-O}) + \nu(\text{Cu-O})$ vibration modes of copper oxalate [20]. The absorption located at 1321 cm^{-1} could be due to $\nu_s(\text{C-O}) + \delta(\text{O-C-O})$ vibration modes of oxalate anion [21,22]. The peak at 1365 cm^{-1} could be ascribed to the $\nu(\text{C-O})$ vibration [20]. The very strong absorption at 1647 cm^{-1} could be due to the $\nu(\text{COO})$ vibration [22], which is in overlap with the bending vibration mode of water [21]. The broad absorption at range of $3000\text{--}3700\text{ cm}^{-1}$ could be attributed to the O-H stretching and bending vibration modes of water molecules [19,23]. Fig. 1(B) shows the XRD patterns of the as prepared RE/Cu oxalates. The X-ray diffraction patterns revealed the crystalline nature of the obtained solids. The strong diffraction peak at 22.94° and the weak ones appearing at the range $2\theta = 35^\circ\text{--}55^\circ$ are similar with those obtained by other research groups [24–26], which can be indexed to the orthorhombic phase of copper oxalate (JCPDS 21–0297, space group Pnm). The various XRD patterns, Fig. 1(B), reveal the presence of other reflections below $2\theta = 21^\circ$. These reflections could reasonably attributed to the presence of the relevant RE oxalates [18].

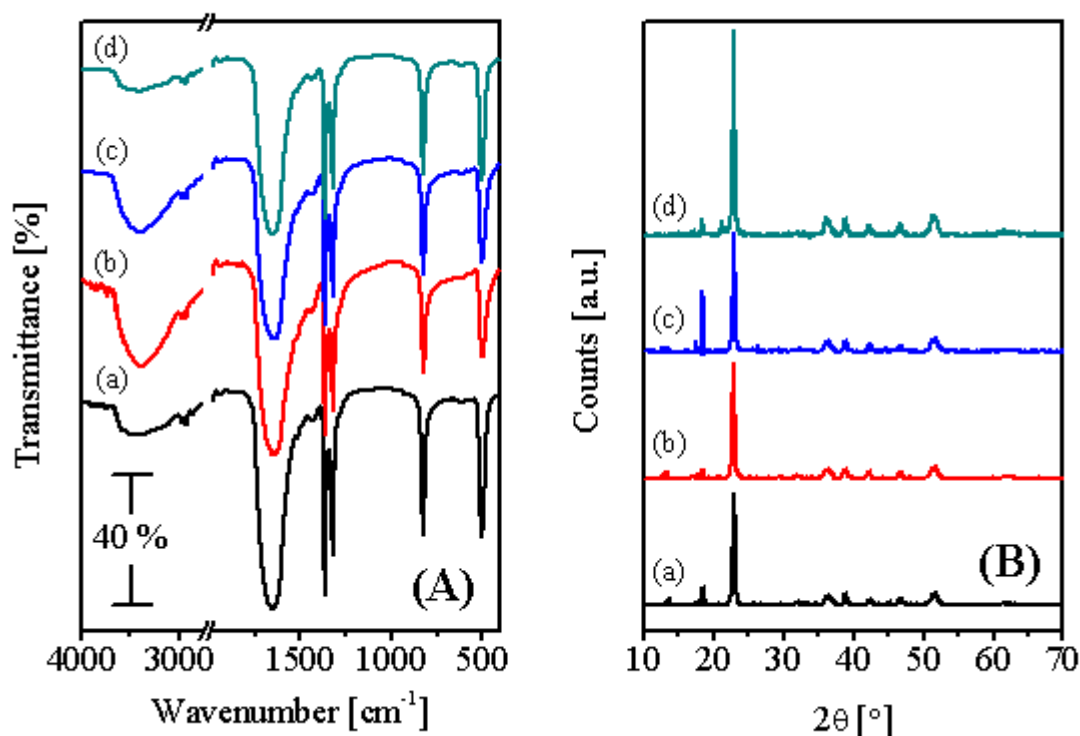


Figure 1. FT-IR spectra (A) and X-ray powder diffraction patterns (B) of Gd/Cu oxalates (a), La/Cu oxalates (b), Nd/Cu oxalates (c), and Y/Cu oxalates (d).

The TGA-DTG thermograms obtained upon heating the various RE/Cu oxalate parents, from ambient till $700\text{ }^\circ\text{C}$ in nitrogen flow, are shown in Fig. 2. Inspection of the obtain thermograms reveals the presence of three weigh loss step, which take place at the temperature ranges of ambient– $100\text{ }^\circ\text{C}$, $150\text{--}325\text{ }^\circ\text{C}$ and $350\text{--}450\text{ }^\circ\text{C}$. The first weight loss could be attributed to the dehydration of the various oxalates. The second step, which is the main step that is maximized at $257\text{--}264\text{ }^\circ\text{C}$, could plausibly

related to the decomposition of copper oxalate [18]. In this context, it was demonstrated that the thermal decomposition of copper oxalate proceeds with the formation of Cu_2O and CuO in an inert and an oxidizing atmospheres, respectively [25,27]. The final weight loss step, which extends over a wide range of temperatures (350–450 °C), could be due to the decomposition of the RE oxalates. Based on the information gathered from Fig. 2 the various RE/CuO catalysts were obtained by the calcination of their relevant oxalate precursors at 500 °C for 1 h in air.

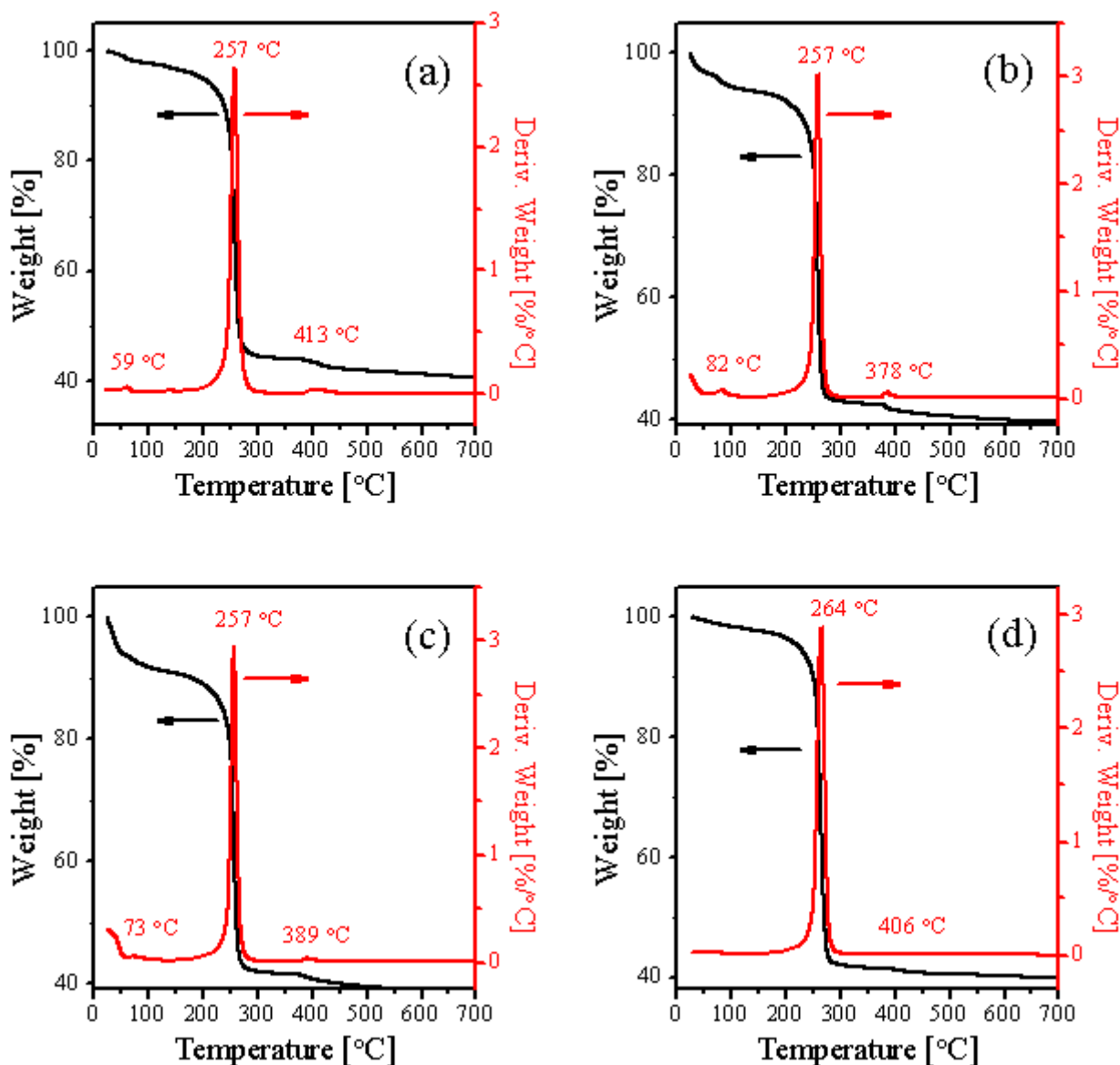


Figure 2. TGA-DTG curves obtained for the Gd/Cu-oxalate (a), La/Cu-oxalate (b), Nd/Cu-oxalate (c), and Y/Cu-oxalate (d).

Room temperature powder XRD patterns obtained for the calcined RE/Cu precursors are shown in Fig. 3(A). Inspection of this figure clearly indicates the disappearance of all reflection due to the presence of oxalate phases observed in Fig. 1(B). Meanwhile new reflections appeared at $2\theta = 32.56^\circ, 35.64^\circ, 38.77^\circ, 48.97^\circ, 53.54^\circ, 58.38^\circ, 61.63^\circ, 66.34^\circ, 68.11^\circ, 72.55^\circ$ and 75.09° . These

reflection can be indexed to a pure monoclinic structure of CuO (space group: Cc) with lattice parameters $a = 4.6893 \text{ \AA}$, $b = 3.4268 \text{ \AA}$, $c = 5.1321 \text{ \AA}$ and $\beta = 99.653$, (JCPDS 80-1917). The obtained pattern for the Gd-containing catalyst indicates the presence of two reflections at $2\theta = 28.57^\circ$ and 47.51° . These two reflections could be assigned to the cubic Gd_2O_3 (JCPDS 76-0155). The diffractogram (b) in Fig. 3(A) show the existence of two reflections at $2\theta = 22.95^\circ$ and 29.51° , which could be assigned to hexagonal La_2O_3 (JCPDS 83-1355). The XRD pattern for Nd-containing catalyst shows the presence of additional reflections at $2\theta = 27.84^\circ$ and 30.10° , which could be ascribed to the presence of hexagonal Nd_2O_3 (JCPDS 83-1353). The XRD pattern for Y/CuO reveals the presence of a reflection at $2\theta = 29.19^\circ$, which could be due to the presence of Y_2O_3 (JCPDS 82-2415). The CuO crystallite sizes of the prepared catalysts were calculated from the XRD line broadening of the diffraction peak at $2\theta = 38.77^\circ$ applying the Scherrer formula [28]. The obtained values (Table 1) ranged between 14 and 19 nm, which are lower than that calculated for bare CuO (53.5 nm) prepared using the same route [18].

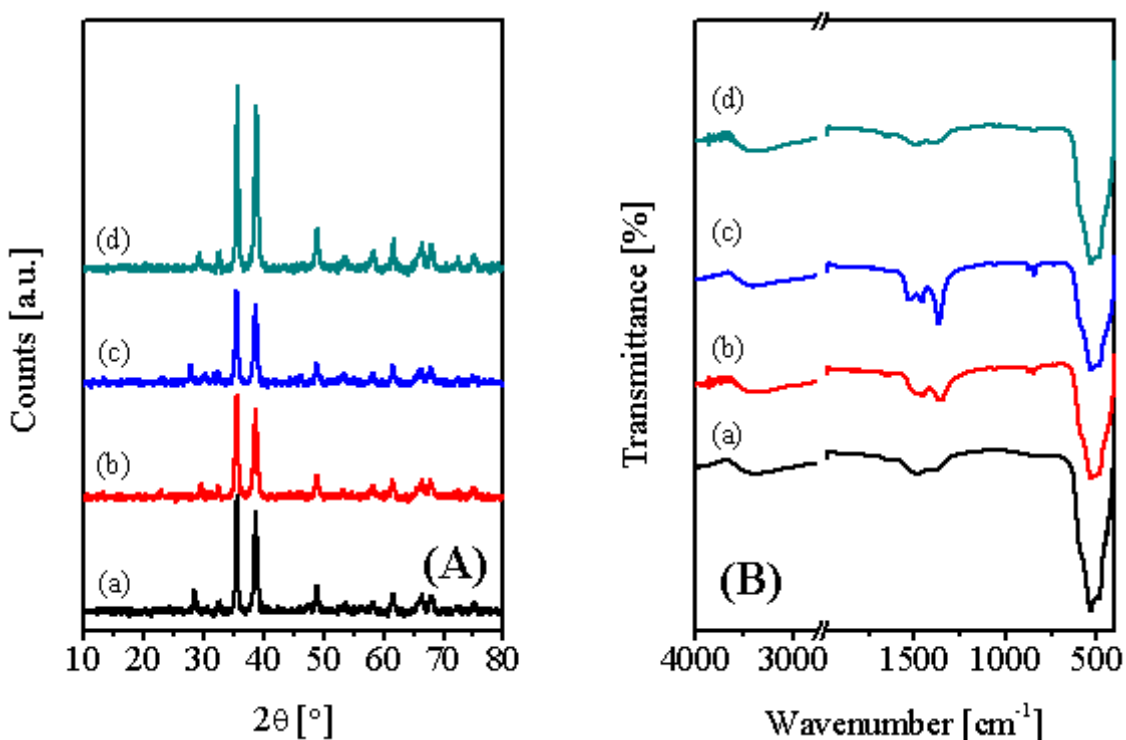


Figure 3. X-ray powder diffraction patterns (A) and FT-IR spectra (B) of Gd/CuO (a), La/CuO (b), Nd/CuO (c), and Y/CuO (d).

Table 1. Crystallite sizes, electrical conductivities, T_{25} and T_{50} values obtained for the RE-promoted CuO catalysts.

Catalyst	Crystallite size [nm]	$\sigma \times 10^{-5} [\Omega^{-1} \text{ cm}^{-1}]$	$T_{25} [^\circ\text{C}]$	$T_{50} [^\circ\text{C}]$
Gd/CuO	17.6	27.4	406	464
La/CuO	14.2	28.6	361	408
Nd/CuO	14.4	20.4	375	434
Y/CuO	19.1	11.2	392	443

Fig. 3(B) shows the FT-IR spectra of the various RE/CuO catalysts. All the obtained spectra indicate the disappearance of all absorptions observed in Fig. 1(A) indicating the complete decomposition of the parent oxalates, which is in a good agreement with the XRD results. Moreover, the spectra in Fig. 3(B) reveal the existence of sharp doublet peak at 480 and 535 cm^{-1} , assignable to the stretching vibrations of CuO ($\text{Cu}^{2+}\text{-O}$) [18,29,30]. The different spectra indicate the presence of other absorptions at 1200–1700 cm^{-1} . Such peaks could be assigned to the carbonate phase. This carbonate species could be formed when the added RE oxides exposed to atmospheric air which leads to the formation of surface carbonates [18,31].

The morphology of the RE/CuO catalysts was analyzed by FE-SEM and the obtained results are shown in Fig. 4. A close inspection of the obtained images reveals that all the obtained catalysts possess the same morphology; they have a sphere-like morphology. These spheres, which have diameters in the range 0.4 μm -2.0 μm , consist of smaller welded spheres with diameters less than 100 nm. Reviewing the recent literature revealed that nanocrystalline CuO can be prepared with various morphologies ranging from 1D ((nanoseeds, nanoribbons and nanowires) to 2D (nanoplates, nanoleaves and nanoflakes) and to 3D (shuttle-like, corncob-like, caterpillar-like, shrimp-like, sphere-like and nanoflowers) [29,32–36]. From the images shown in Fig. 4 it is obvious that by employing the microwave assisted precipitation route for the preparation of RE-promoted CuO catalysts leads to the formation of solids with a sphere-like morphology. Moreover, from the combination of the obtained images and that of the bare CuO, prepared using the same route [18], it seems that the presence of the added RE oxides does not hinder the formation of the CuO with sphere-like morphology. However, the presence of such dopant leads to a decrease of the size of the formed spheres. This finding agrees well with the XRD results.

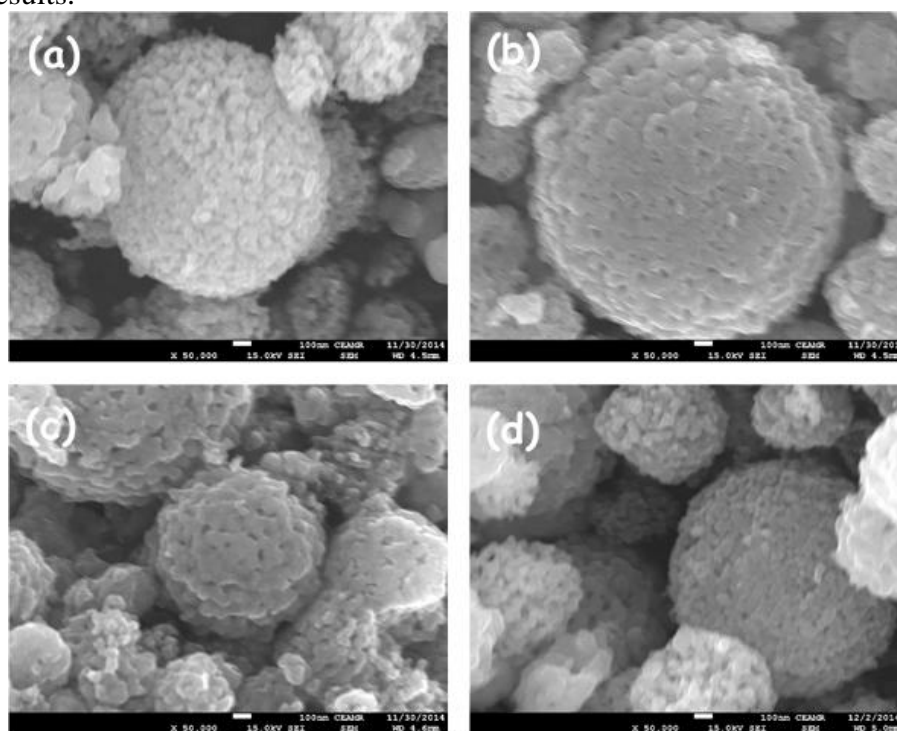


Figure 4. FE-SEM images obtained for Gd/CuO (a), La/CuO (b), Nd/CuO (c) and Y/CuO (d) catalysts.

Fig. 5 depicts typical TEM images, with the same magnification, obtained for the RE/CuO catalysts. Close inspection of these images indicates that these catalysts are composed of uniform crystallites that possess a sphere-like or polygonal morphology with diameters ranging between 15 to 40 nm. Such values are close to those determined by the XRD analysis. The small crystallites are welded together forming spherical aggregates, which is obvious in case of La/CuO catalyst (image (b)). In this context, it is to be mentioned that the TEM-estimated crystallites sizes of the various RE/CuO catalysts are smaller than that of bare CuO (80-160 nm) [18].

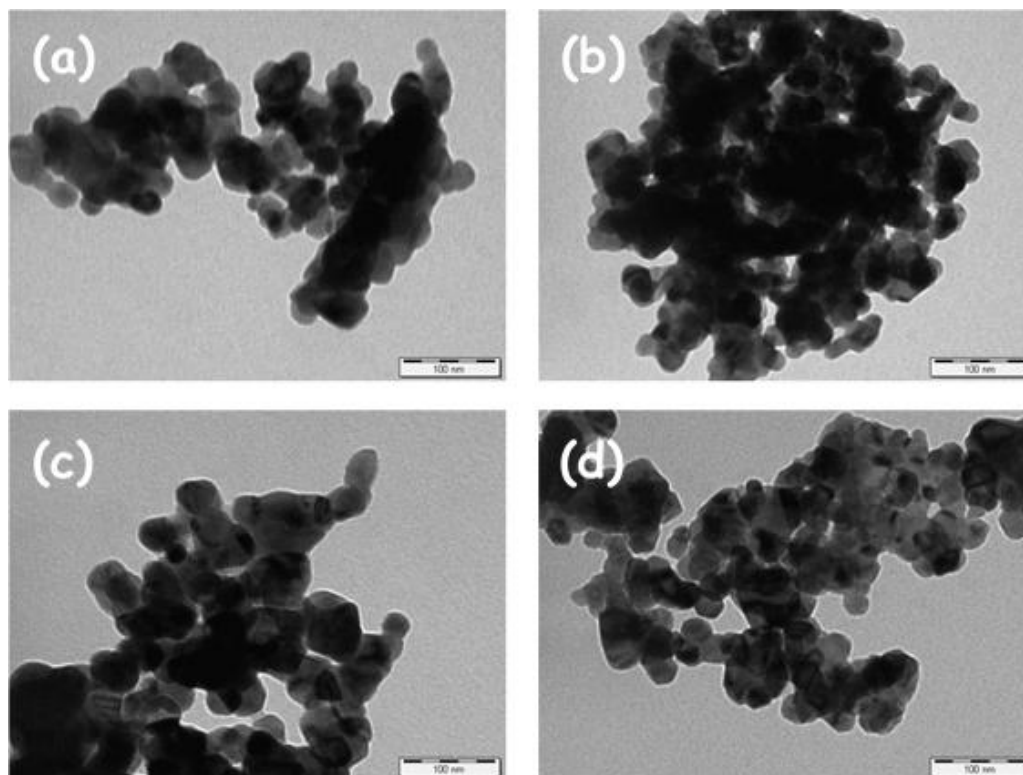


Figure 5. TEM nano-graphs obtained for Gd/CuO (a), La/CuO (b), Nd/CuO (c) and Y/CuO (d) catalysts.

Fig. 6 shows N_2 adsorption-desorption isotherms, measured at $-196\text{ }^\circ\text{C}$, for the different calcined RE/CuO catalysts. The obtained isotherm for bare CuO belongs to Type III of the nitrogen adsorption isotherms classification with adsorption branch laying on the desorption one [37]. The calculated BET surface area of this catalyst is $3.2\text{ m}^2/\text{g}$ (Table 2). The obtained isotherms for the RE-promoted CuO are still showing the Type III character but with the development of hysteresis loops at the range of $P/P_0 = 0.85-0.90$. All the RE-promoted catalysts showed higher BET surface area and pore volume values compared to those of the bare CuO (Table 2).

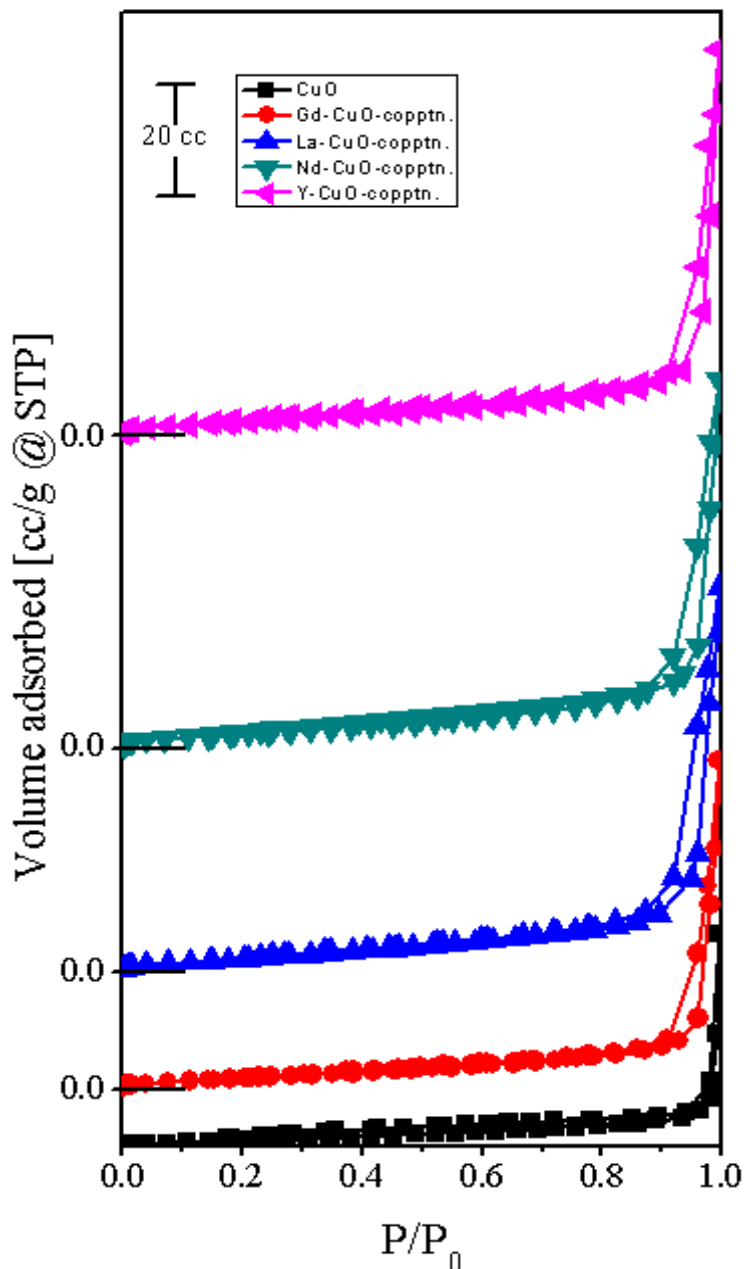


Figure 6. Nitrogen adsorption-desorption isotherms obtained for bare CuO and it RE-containing catalysts.

Table 2. Texture data of CuO based catalysts prepared by the co-precipitation method.

Catalyst	S_{BET} [$m^2 g^{-1}$]	V_p [$cc g^{-1}$]	P_d [nm]
CuO	3.2	0.057	3.367
Gd/CuO	6.3	0.089	3.078
La/CuO	9.9	0.105	3.670
Nd/CuO	8.9	0.100	3.044
Y/CuO	8.9	0.104	3.979

S_{BET} = BET surface area, V_p = pore volume, and P_d = pore diameter

In order to gain more information about the Cu-surface species in the bare CuO and its RE-containing catalysts, the chemical compositions of the CuO and La/CuO catalysts were investigated by using X-ray photoelectron spectroscopy.

Table 3. Cu 2p_{3/2} and O 1s binding (eV) energies of CuO and La/CuO catalysts.

Catalyst	Cu ⁺	Cu ⁺⁺	O ²⁻ in CuO	O ²⁻ in Cu ₂ O, CuO or Cu(OH) ₂	C-O
CuO	932.7	933.95	529.28	530.81	533.48
La/CuO	932.67	934.62	529.08	530.91	533.14

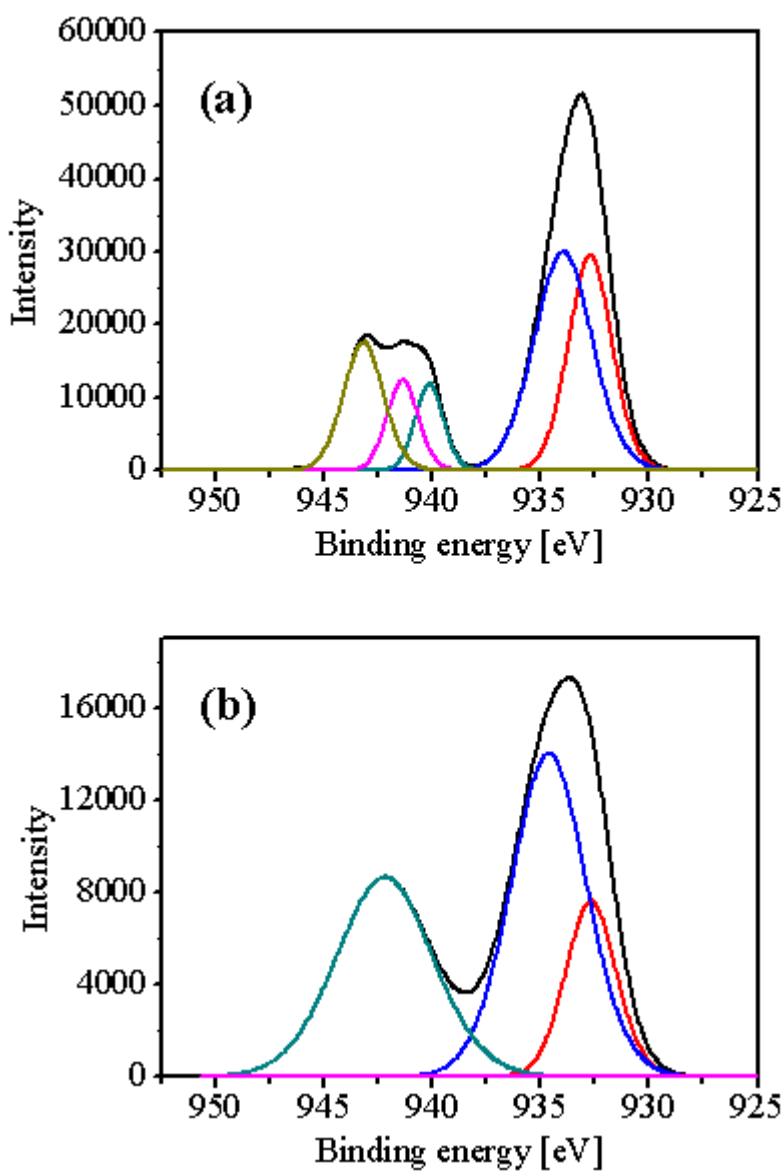


Figure 7. Cu 2p_{3/2} XPS spectra of CuO (a) and La/CuO (b) catalysts.

Fig. 7 shows the Cu $2p_{3/2}$ XPS spectra of CuO and La/CuO catalysts. The spectra were calibrated by using the binding energy (BE) 284.5 eV of C1s electron. The $2p_{3/2}$ peak of bare CuO (Fig. 7(a)) can be deconvoluted into two peaks at 932.70 and 933.95 eV (Table 3). These two contributions could be assigned to Cu^+ and Cu^{++} species on the CuO surface, respectively [38–41]. The deconvoluted spectrum of the Cu $2p_{3/2}$ XPS spectrum of La/CuO catalyst (Fig. 7(b)) shows two contributions at 932.67 and 934.62 eV, which indicate the presence of Cu^+ and Cu^{++} species on the surface of this catalyst too. The slight shift of the Cu^+ binding energy (BE) upon adding La to CuO indicates that this Cu^+ species has higher ability to give electrons giving Cu^{++} one compared to bare CuO. On the other hand, the higher BE of Cu^{++} contained in the La/CuO compared to bare CuO is a major characteristic of oxidized Cu^{++} species [40], i.e. easier to be reduced Cu^{++} species.

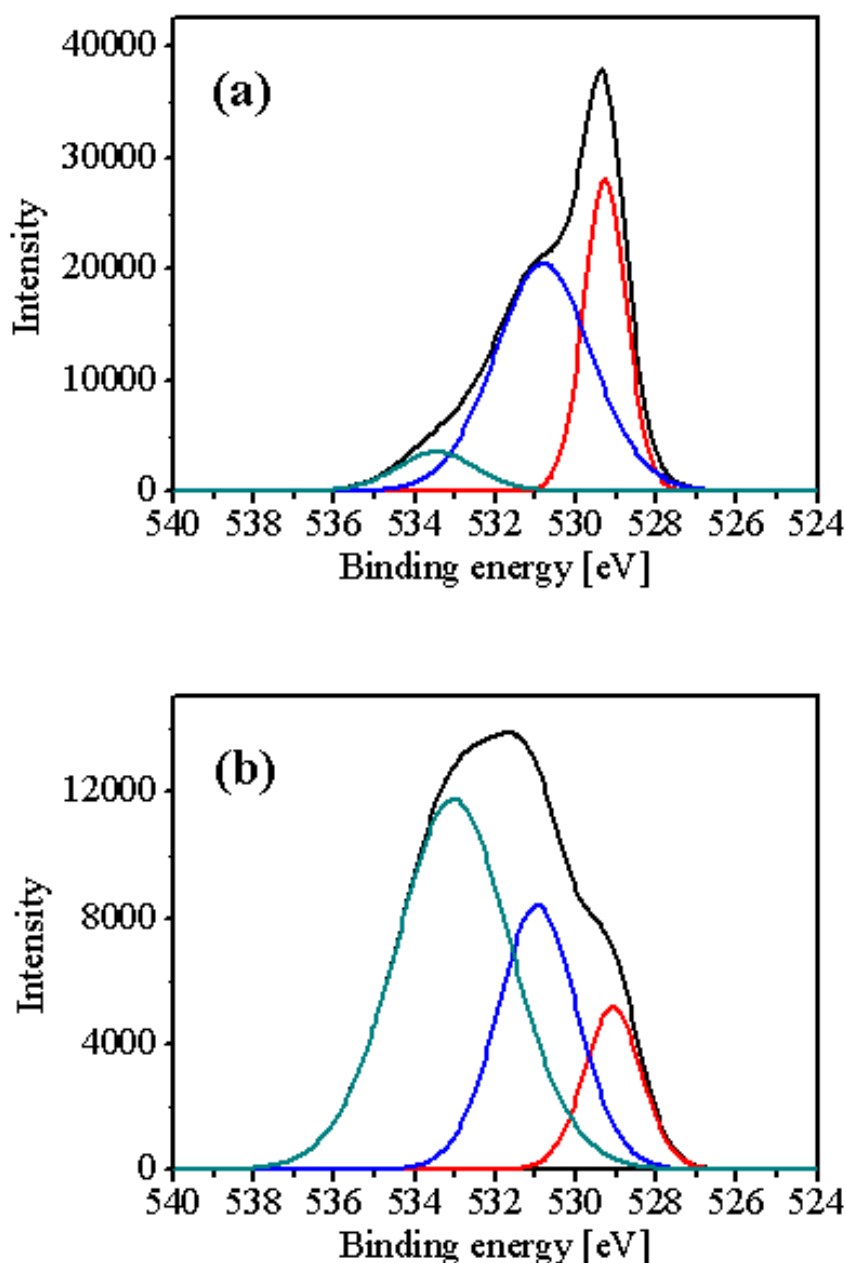


Figure 8. O 1s XPS spectra of CuO (a) and La/CuO (b) catalysts.

The O 1s core level spectra, Fig. 8, show an asymmetric BE peak due to two contributions. This surface O1s peak of bare CuO (Fig. 8(a)) can be fitted into three peaks centered at 529.28, 530.81 and 533.48 eV. The contribution at 529.28 eV corresponds to lattice oxygen O^{2-} of CuO, whereas the peak at 530.81 eV could be assigned to lattice O^{2-} of Cu_2O , CuO or $Cu(OH)_2$ [38,41]. The highest BE peak at 533.48 eV can be assigned to C–O species [41], which could be attributed to the presence of surface carbonate species. Similar picture can be observed for the La/CuO catalyst (Fig. 8(b)). However, sharp increase in the intensity of the surface carbonate species can be observed. This can be correlated with the presence of surface carbonate species as a result of La-doping as indicated during the discussion of FT-IR results (Fig. 3(b)).

3.2. N_2O decomposition activity

Fig. 9 shows the variation of the percent N_2O conversion as a function of reactor temperature on bare CuO as well as its RE-containing catalysts. Comparisons of the activity profiles were conducted under the same reaction conditions, as described in the experimental part. In the whole temperature range investigated (225–500 °C), all tested catalysts were active and their activity increases with the reactor temperature. Table lists the T_{25} and T_{50} values (temperature of 25 and 50 % conversion, respectively) of the tested catalysts. From the data presented in Fig. 9 and Table 1, it is obvious that all the RE-containing catalysts show higher activity compared to the bare CuO one. The obtained activity order is bare CuO < Gd/CuO < Y/CuO < Nd/CuO < La/CuO. It is worth mentioning that the N_2O decomposition experiments over bare RE-oxides reveals their very low activity; less than 5 % conversion was obtained at a reactor temperature of 500 °C.

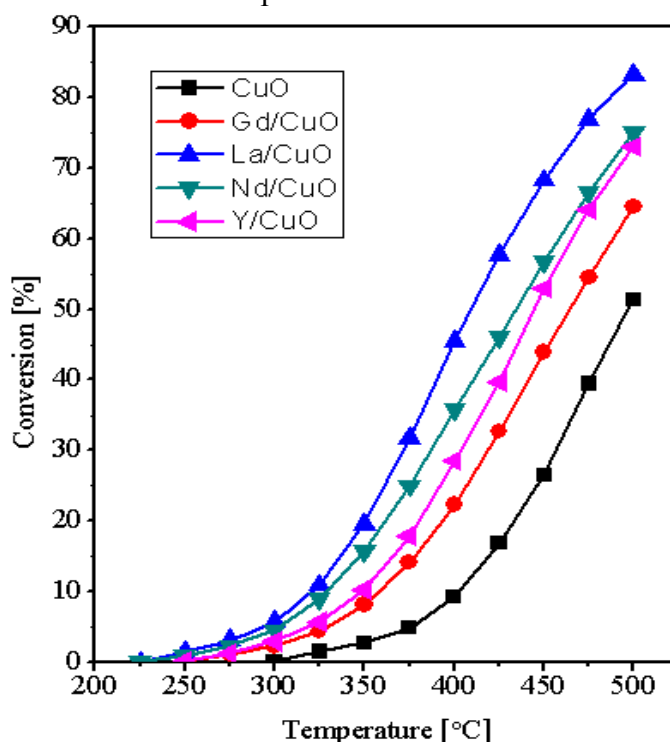


Figure 9. Percent N_2O conversion as a function of reactor temperature on bare CuO, Gd/CuO, La/CuO, Nd/CuO, and Y/CuO catalysts.

In the open literature, there are many papers reporting the promotion effect of dopants, usually alkali cations, on the activity of N₂O direct decomposition of various catalysts [5,6,10,17,18,42–46]. Only little authors have reported the role of cations doping in enhancing the N₂O decomposition over CuO catalysts [9,17,45]. For instance, Pasha et al. [9] reported the enhancement effect of Cs-ions doping of CuO, where the highest activity was observed on the catalyst with Cs/Cu ratio of 0.1. Promotion effect during N₂O decomposition over CuO was, also, reported on doping with Ce-ions [17,45].

The activity enhancement for N₂O direct decomposition of the added promoters can be understood based on the variation of the electrical properties of the catalysts. In this way, the activity of *p*-type semiconductors was found to be superior to that of the *n*-type semiconductors or insulator [2]. Based on in situ electrical conductivity measurements, the high N₂O decomposition activity of Fe-, Co-, Cu-, Pd-, La-, Ce- and Ag-ZSM-5 [15] and Cu-X zeolite catalysts [16] was correlated with their ability to show high magnitude of electrical conductivity lowering upon the admission of N₂O. More recently, we have correlated the activity enhancement on doping CuO with Pr₆O₁₁, Tb₄O₇ and Sm₂O₃ with the obtained conductivity as well as reduction enhancement [18]. The reported N₂O decomposition mechanism over many solid catalysts requires the existence of Mⁿ⁺/Mⁿ⁺¹ redox couple [5,15–17]. In the preceding section, we have observed, based on XPS analysis, the coexistence of Cu⁺ and Cu²⁺ on bare CuO as well as its La-containing catalyst. Accordingly, we may suggest a reaction mechanism similar to that reported for other oxide-based catalysts as follows:



Similar reaction mechanism was suggested for N₂O decomposition over CeO₂-CuO catalysts [17] and for N₂O oscillation on Cu-ZSM-5 [47]. During the first step in this mechanism an electron donation occurs from the catalyst surface to N₂O molecule, which results in its adsorption. This step leads to the charge transfer to N₂O forming and adsorbed N₂O⁻ and the oxidation of Cu⁺ ion to Cu²⁺ one. The second step includes an evolution of N₂ molecule and formation of adsorbed oxygen atom. The final step involves a liberation of oxygen and the regeneration of the catalyst active center, i.e. Cu⁺. It was shown that the added promoters improves the electron donation ability of the catalysts active centers [5,6,17,18]. Comparing the obtained electrical conductivity values of the various RE/CuO catalysts (Table 1) with that of bare CuO, 2.0 × 10⁻⁵ (Ω⁻¹ cm⁻¹) [18], reveals their higher conductance. Our XPS analysis (Fig. 7 and Table 3) revealed a shift in the 2P_{3/2} peak of Cu⁺ towards lower BE for La/CuO compared to bare CuO, which indicates the higher ability of the former catalyst to give electron and being oxidized. In this context, Asano et al. [48] showed that potassium doping of Co₃O₄ catalyst has led to a slight decrease in the BE of the Co 2p_{3/2} XPS-peak. Recently, a shift in the Ni 2p_{3/2} XPS-peak of Ni⁰ was reported as a result of doping NiO with K ions [49]. These BE shifts have been suggested to be responsible for the sharp increase in the N₂O-decomposition reactivity K-doped Co₃O₄ and NiO catalysts [48,49]. From the combination of our results with these literature data it is reasonable to suggest that the added RE promoters would favor the formation of a surface electron-rich Cu⁺ species. These species have greater ability for electron donation to the coming N₂O

molecules, thus favoring their adsorption on the catalyst surface. This, in turn, would result in the formation of adsorbed N_2O^- and the $Cu^+ \rightarrow Cu^{2+}$ transformation (equation 1).

In order to understand the role of the added RE-oxides in enhancing the recoverability of the Cu^+ species we have carried out a series of H_2 -TPR experiments. Fig. 10 shows the H_2 -TPR profiles for bare CuO and its Gd-, La, Nd, and Y-containing catalysts. These profiles are characterized by the presence of only one broad peak covering a wide range of temperatures. With the aid of other literature data [17,40], this peak could be related to two reduction processes, as follows:

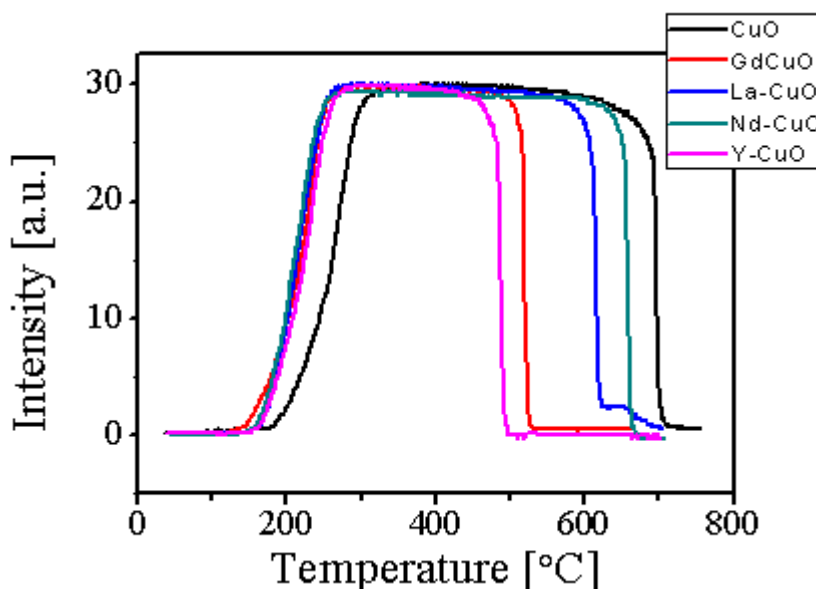
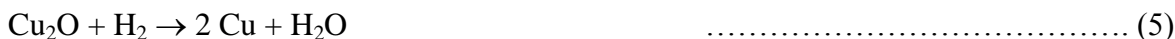


Figure 10. TPR profiles obtained for CuO, Gd/CuO, La/CuO, Nd/CuO and Nd/CuO catalysts.

From the data presented in Fig. 10 it is obvious that all the RE-ions shift the H_2 -TPR peak towards lower temperatures. This, in turn, suggests that the addition of the RE-oxides to CuO enhances its reducibility. This finding agrees well with the observed shift in the $2P_{3/2}$ peak of Cu^{++} towards higher values upon the addition of La-ions (Table 3), which indicates the improved reducibility of CuO. This improved CuO reducibility facilitates the recoverability of the adsorption active centers, i.e. Cu^+ ions. This means that, the rate of reaction step no. 3 will increase on doping CuO with some RE-oxides. In other words, the added RE-oxides enhance the recoverability of the catalysts active centers, and thus increasing the N_2O decomposition activity. In this context, the N_2O decomposition activity could be influenced by other parameters including the BET surface area and the catalysts crystallites sizes. Over metal oxide-based catalysts, it was shown that the activity increases with the $S_{E_{BT}}$ increase and the decrease in the catalysts crystallite sizes [5,6,28,50]. From the preceding section, it was shown that the addition of RE-oxides to CuO leads to an increase in its BET surface area and a decrease in its crystallites size. Therefore, these two parameters could be additional factors that could participate in the activity enhancement upon the incorporation of RE-oxides into CuO.

4. CONCLUSIONS

The catalytic activity for N₂O decomposition was tested over of RE-promoted CuO catalysts, prepared by the microwave assisted co-precipitation method, and compared to that of bare CuO. The results obtained clearly revealed that the RE-promoted catalysts exhibit better catalytic performance compared to the un-promoted CuO. This improved activity of the RE/CuO catalysts was correlated with the role of the added RE-oxides in enhancing the electrical conductivity as well as the Cu⁺/Cu⁺⁺ redox cycle on the surface of CuO, which facilitate the oxygen desorption from the catalysts surfaces. Moreover, it was suggested that the active sites in the RE/CuO catalysts are more accessible due to their higher surface area and lower crystallite sizes.

ACKNOWLEDGEMENTS

This project was supported by the National Science, Technology and Innovation Plan (MAARIFAH) strategic technologies programs, number (12-ENV2756-03) of the Kingdom of Saudi Arabia. The authors thankfully acknowledge Science and Technology Unit, Deanship of Scientific Research at King Abdulaziz University for their technical support.

References

1. J. Pérez-Ramírez, *Appl. Catal. B*, 70 (2007) 31.
2. R. M. Dell, F. S. Stone and P. F. Tiley, *Trans. Faraday Soc.*, 49 (1953) 201.
3. T. Yamashita and M. Avannice, *J. Catal.*, 161 (1996) 254.
4. F. Kapteijn, J. Rodriguez-Mirasol and J. A. Moulijn, *Appl. Catal. B*, 9 (1996) 25.
5. B. M. Abu-Zied and S. A. Soliman, *Catal. Lett.*, 132 (2009) 299.
6. B. M. Abu-Zied, S. A. Soliman and S. E. Abdellah, *J. Ind. Eng. Chem.*, 21 (2015) 814.
7. S. Tuti, F. Pepe, D. Pietrogiamomi and V. Indovina, *React. Kinet. Catal. Lett.*, 72 (2001) 35.
8. K.-W. Yao, S. Jaenicke, J.-Y. Lin and K. L. Tan, *Appl. Catal. B.*, 16 (1998) 291.
9. N. Pasha, N. Lingaiah, P. S. S. Reddy and P.S. Sai Prasad, *Catal. Lett.*, 127 (2009) 101.
10. N. Pasha, N. Lingaiah, P. S. S. Reddy, P. S. Sai Prasad, *Catal. Lett.*, 118 (2007) 64.
11. L. M. Madeira, J. M. Herrmann, F. G. Freire, M. F. Portela and F. J. Maldonado, *App. Catal. A*, 158 (1997) 243.
12. P. Viparelli, P. Ciambelli, J.-C. Volta and J.-M. Herrmann, *App. Catal. A*, 182 (1999) 165.
13. B. M. Abu-Zied and A. M. El-Awad, *J. Mol. Catal. A*, 176 (2001) 227.
14. I. Popescu, Y. Wu, P. Granger and I.-C. Marcu, *App. Catal. A*, 485 (2014) 20.
15. B. M. Abu-Zied, W. Schwieger and A. Unger, *App. Catal. B*, 84 (2008) 277.
16. B. M. Abu-Zied, *Microporous Mesoporous Mater.*, 139 (2011) 59.
17. M. Konsolakis, S. A. C. Carabineiro, E. Papista, G. E. Marnellos, P. B. Tavares, J. A. Moreira, Y. Romaguera-Barcelay and J. L. Figueiredo, *Catal. Sci. Technol.*, 5 (2015) 3714.
18. B. M. Abu-Zied, S. M. Bawaked, S. A. Kosa and W. Schwieger, *Int. J. Electrochem. Sci.*, 11 (2016) in press.
19. B. M. Abu-Zied, S. M. Bawaked, S. A. Kosa and W. Schwieger, *Appl. Surf. Sci.*, 351 (2015) 600.
20. M. C. D'Antonio, D. Palacios, L. Coggiola and E. J. Baran, *Spectrochim. Acta Part A*, 68 (2007) 424.
21. M. C. D'Antonio, N. Mancilla, A. Wladimirsky, D. Palacios, A. C. González-Baró and E. J. Baran, *Vib. Spectrosc.*, 53 (2010) 218.

22. D. Palacios, A. Wladimirsky, M. C. D'Antonio, A. C. González-Baró and E. J. Baran, *Spectrochim. Acta Part A*, 79 (2011) 1145.
23. B. M. Abu-Zied, A.A.A. Farrag and A. M. Asiri, *Powder Technol.*, 246 (2013) 643.
24. D. X. Zhang, H. Xu, Y. Z. Liao, H. S. Li and X. J. Yang, *Powder Technol.*, 189 (2009) 404.
25. E. Lamprecht, G. M. Watkins and M. E. Brown, *Thermochim. Acta*, 446 (2006) 91.
26. W. Kang and Q. Shen, *J. Power Sources*, 238 (2013) 203.
27. A. Aimable, A. T. Puentes and P. Bowen, *Powder Technol.*, 208 (2011) 467.
28. B. M. Abu-Zied, *Appl. Catal. A*, 334 (2008) 234.
29. B. Shaabani, E. Alizadeh-Gheshlaghi, Y. Azizian-Kalandaragh and A. Khodayari, *Adv. Powder Technol.*, 25 (2014) 1043.
30. J. K. Sharma, M. S. Akhtar, S. Ameen, P. Srivastava and G. Singh, *J. Alloys Compd.*, 632 (2015) 321.
31. S.A. Soliman and B.M. Abu-Zied, *Thermochim. Acta*, 491 (2009) 84.
32. J. Liu, J. Jin, Z. Deng, S.-Z. Huang, Z.-Y. Hu, L. Wang, C. Wang, L.-H. Chen, Y. Li, G. Van Tendeloo and B.-L. Su, *J. Colloid Interface Sci.*, 384 (2012) 1.
33. T. Jiang, Y. Wang, D. Meng, X. Wu, J. Wang and J. Chen, *Appl. Surf. Sci.*, 311 (2014) 602.
34. G. Bozkurt, A. Bayrakçeken and A. K. Özer, *Appl. Surf. Sci.*, 318 (2014) 244.
35. J.-H. Kim, A. Katoch, S.-W. Choi and S. S. Kim, *Sens. Actuators B*, 212 (2015) 190.
36. Z. Jia, L. Yue, Y. Zheng and Z. Xu, *Mater. Res. Bull.*, 43 (2008) 2434.
37. P.A. Webb and C. Orr, *Analytical Methods in Fine Particles Technology*, Micromeritics Instrument Corp., 1997, p. 55.
38. B. Heng, C. Qing, H. Wang, D. Sun, B. Wang and Y. Tang, *J. Alloys Compd.*, 649 (2015) 899.
39. J. M. L. Martínez, E. Rodríguez-Castellón, R. M. T. Sánchez, L. R. Denaday, G. Y. Buldain and V. C. Dall'Orto, *J. Mol. Catal. A*, 339 (2011) 43.
40. Q. Zhang, L. Xu, P. Ning, J. Gu and Q. Guan, *Appl. Surf. Sci.*, 317 (2014) 955.
41. J. Demel, A. Zhigunov, I. Jirka, M. Klementová and K. Lang, *J. Colloid Interface Sci.*, 452 (2015) 174.
42. J. Haber, T. Machej, J. Janas and M. Nattich, *Catal. Today*, 90 (2004) 15.
43. J. Haber, M. Nattich and T. Machej, *Appl. Catal. B*, 77(2008) 278.
44. G. Maniak, P. Stelmachowski, A. Kotarba, Z. Sojka, V. Rico-Pérez and A. Bueno-López, *Appl. Catal. B*, 136-137 (2013) 302.
45. A. Adamski, W. Zajac, F. Zasada and Z. Sojka, *Catal. Today*, 191 (2012) 129.
46. A. Klyushina, K. Pacultová, S. Krejčová, G. Słowik, K. Jiráková, F. Kovanda, J. Ryczkowski and L. Obalová, *Catal. Today*, 257 (2015) 2.
47. P. Ciambelli, A. Di Benedetto, E. Garufi, R. Pirone and G. Russo, *J. Catal.*, 175 (1998) 161.
48. K. Asano, C. Ohnishi, S. Iwamoto, Y. Shioya and M. Inoue, *Appl. Catal. B*, 78 (2008) 242.
49. B. M. Abu-Zied and A. M. Asiri, *Chin. J. Catal.*, 36 (2015) 1837.
50. B. M. Abu-Zied, S. A. Soliman and S. E. Abdallah, *Chin. J. Catal.*, 35 (2014) 1105.